

## High spatial resolution X-ray spectroscopy of SNR Cassiopeia A with *Chandra*

Xue-Juan Yang<sup>1,2\*</sup>, Fang-Jun Lu<sup>1</sup> and Li Chen<sup>2</sup>

<sup>1</sup> Particle Astrophysics Center, Institute of High Energy Physics, Chinese Academy of Sciences, Beijing 100049, China

<sup>2</sup> Department of Astronomy, Beijing Normal University, Beijing 100875, China

**Abstract** We present high spatial resolution X-ray spectroscopy of supernova remnant Cassiopeia A with the *Chandra* observations. The X-ray emitting region of this remnant was divided into  $38 \times 34$  pixels with a scale of  $10'' \times 10''$  each. Spectra of 960 pixels were created and fitted with an absorbed two component non-equilibrium ionization model. With the spectral analysis results we obtained maps of absorbing column density, temperatures, ionization ages, and the abundances for Ne, Mg, Si, S, Ca and Fe. The Si, S and possibly Ca abundance maps show obviously jet structures, while Fe doesn't follow the jet but seems to be distributed perpendicular to it. In the range of about two orders of magnitude, the abundances of Si, S and Ca show tight correlations between each other, suggesting them to be ejecta from explosive O-burning and incomplete Si-burning. Meanwhile, Ne abundance is well correlated with that of Mg, indicating them to be the ashes of explosive C/Ne burning. The Fe abundance is positively correlated with that of Si when Si abundance is lower than 3 solar abundances, but a negative correlation appears when the Si abundance is higher. We suggest that such a two phase correlation is the results of different ways in which Fe is synthesized.

**Key words:** ISM: supernova remnants – ISM: individual: Cassiopeia A

## 1 INTRODUCTION

The young core-collapse supernova remnant (SNR) Cassiopeia A (Cas A) is a perfect laboratory for studying the ejecta and shock in remnants, for its age and distance are well-determined and it is very bright across the whole electromagnetic spectrum. The age of Cas A is around 300 years (Thorstensen et al. 2001) and the distance about 3.4 kpc (Reed et al. 1995). It appears today as a nearly circular 3 arcmin diameter bright ring, with a low surface brightness 5 arcmin diameter radio and X-ray plateau. As a young SNR, it is believed that thermal X-ray emission mainly comes from the forward shocked interstellar medium (ISM) (Shklovsky 1973) and the reverse shocked supernova (SN) ejecta (McKee 1974). The X-ray image of Cas A is consistent with this scenario as suggested by Gotthelf et al. (2001). They discovered a thin, bright X-ray wisp that is interpreted as the forward shock, and a sharp rise in radio and X-ray line emissivity at the inner edge of the bright ring, which is associated with the reverse shock.

Numerical models (e.g., Woosley & Weaver 1995; Thielemann et al. 1996) predict that nucleosynthesis in core-collapse supernovae (SNe) occurs in an “onionskin” manner. Explosive Si burning occurs near the core, where the shock temperatures is the highest. This process would burn up Si and form ejecta dominated by  $^{56}\text{Ni}$ , which decays to  $^{56}\text{Co}$  and finally  $^{56}\text{Fe}$ . Further out, as the shock temperature decreases, Si burning is incomplete and the main products include not only Fe, but also much Si, S, Ar and Ca. Even further out, explosive O burning occurs, leading to a composition dominated by O and Si with very little or no Fe. At the outmost the explosive Ne/C burning occurs and forms mostly O. Willingale et al. (2002) did a spectral mapping of Cas A using the data collected by the XMM-Newton X-ray observatory (*XMM-Newton*). They found that the distributions of Si, S, Ar and Ca are very similar to each other but distinct from Ne and Mg. This supports the above explosive nucleosynthesis network. However, Hughes et al. (2000) and Willingale et al. (2002) showed that the Fe-rich ejecta lie outside the Si-rich material, using data from the Chandra X-ray observatory (*Chandra*) and *XMM-Newton* respectively. It was concluded that the ejecta in Cas A have undergone a spatial inversion of the explosive O- and Si-burning products. That is to say, the materials from the predicted “onion” layers have mixed together. Hughes et al. (2000) proposed this inversion to be the result of neutrino-driven convection during the initiation of the SN explosion.

*Chandra* performed a 1 Ms observation on Cas A as a Very Large Project (VLP), which was largely motivated by the two papers: Laming & Hwang (2003) and Hwang & Laming (2003), focusing on the suggested jet structure of the ejecta and the iron synthesis. Hwang et al. (2004) showed the first sight of the observation. A jet structure of the Si-rich ejecta was clearly found in the en-

---

\* E-mail: yangxj@mail1.ihep.ac.cn

hanced Si-K emission line image. So it is proposed that Cas A was formed by an asymmetric explosion, which is also indicated by the observed kinematics and the high  $^{44}\text{Ti}$  yield (Vink 2004). Fe-rich ejecta, however, was not found in the jet area, but perpendicular to it instead. This contradicts to jet-induced explosion (Khokhlov et al. 1999), but might be the case for collapsars (Nagataki et al. 2003; Zhang et al. 2004). The explosion energy for Cas A was about  $2 \sim 4 \times 10^{51}$  ergs, suggesting it to be a normal SN (Laming & Hwang 2003). Cas A thus provides strong evidence that jets may also be produced by normal SNe (Hwang et al. 2004).

In this paper, we present high resolution X-ray spectroscopy of Cas A using the *Chandra* observations. Willingale et al. (2002) did a similar work with the *XMM-Newton* data. Here we would like to cross-check their results. In our work, we use a smaller pixel size ( $10'' \times 10''$ , 1/4 of that used by Willingale et al. (2002)), which is closer to the typical size of the ejecta knots of Cas A. Another point is that the so-called “jet” region is included in the analysis, while not in Willingale et al. (2002). The high spatial and spectral resolutions of *Chandra* together with the abundant archived data permit us to study this famous SNR in detail. In § 2, we briefly describe the observation and data reduction. In § 3, we show the results, while some discussion in § 4, and summary in § 5.

## 2 OBSERVATION AND DATA REDUCTION

Cas A was observed by *Chandra* for about 1 Ms in 2004 as a VLP. The details of the observations were described by Hwang et al. (2004). In this paper, we used data from two deep ACIS exposure segments of the VLP. One was performed from April 14 to 16 (Observation ID: 4638) and the other from May 25 to 26 (Observation ID: 4639), with the exposure time of about 167 ks and 80 ks respectively. The reasons that we used two segments are to ensure good statistic for the spatially resolved analysis and to reduce the mis-calibration effects, by using data collected in different epochs.

The X-ray data were analyzed using CIAO software package (version 3.3, with the CALDB version 3.2.1 and the ATOMDB version 1.3.1). In order to do spatially resolved analysis, the X-ray emission region was divided into pixels with size about  $10'' \times 10''$ , corresponding to a grid of  $38 \times 34$ . Figure 1 shows the image for observation ID 4639 with the grid overlaid. We retained events within energies 0.5-10 keV using the archived level 2 event file and created spectra for 960 pixels that contain at least 3000 counts. The frequency distribution of the counts in each pixel is shown in Figure 2 (left panel). We can see that most pixels contain more than 10000 counts, which allows statistical reliable spectral analysis. The background spectrum was created from the off-source region.

The spectral analysis was performed using the XSPEC (version 11.2) package (Arnaud 1996). The spectra for each pixel of the two observations were jointly fitted with two non-equilibrium ionization components (VNEI, Borkowski et al. 2001). The free parameters are the temperatures, emission measures, ionization ages ( $\tau = n_e t$ ) and abundances of O, Ne, Mg, Si, S, Ca and Fe for each of the two components. The abundances are in units of solar abundances given by Anders & Grevesse (1989). We also introduced a uniform redshift for each component to study the dynamics. The WABS model (Morrison & MacCammon 1983) was included to take care of interstellar photo-electric absorption. A Gaussian line was added at the energy of 3.4 keV to account for the Ar line emission, which is not included in the VNEI model in XSPEC version 11.2 we used.

Here we note two points. One is that the nonthermal emission contributes to the 4 ~ 6 keV continuum without any doubt, which could be as high as 25% in Cas A (Willingale et al. 2002). However, since its X-ray emission is dominated by the thermal component (Laming 2001; Bleeker et al. 2001) and we are mainly interested in the study of line emission in this paper, we believe that our model is appropriate. The same spectral model was also used by Willingale et al. (2002). The other is that Cas A is an O-rich SNR, so that O contributes a significant fraction of the electrons (Vink et al. 1996; Willingale et al. 2002). In this case, the O abundance is coupled with the emission measure. Here we set the O abundances of both components free in the fitting process, but we will not discuss about the O abundance in this paper as it might be contaminated.

### 3 RESULTS

The frequency distribution of the 960 reduced  $\chi^2$  values of the spectral fits is given in Figure 2 (right panel). It has a peak around 0.7, which suggests our fitting results to be acceptable statistically. In Figure 3, we give the spectra along with the fitting residuals of several typical regions (marked in Figure 1). The emission lines are also marked. Region A is located at the outmost of the jet in the northeast. It has very strong Si, S, Ar and Ca lines, but the Fe-K line is absent. Therefore it should be dominated by O-burning products, but we cannot rule out the incomplete Si-burning, as there seem to be the Fe-L lines around 1 keV (c.f. § 1). Region B is from the counter-jet, which is very strong in Si and S. The Fe-K line is also clearly shown. This is very consistent with the incomplete Si-burning yield out. Region C is the Fe-rich region from the southeast. From the spectra we can see very strong Fe-K and Fe-L lines, which are believed to be from complete explosive Si-burning. Region D is located at the out rim, which is weak in all the emission lines of the main elements in Cas A and dominated by the continuum (c.f. Hughes et al. 2000, Figure 3). These spectra show that the

X-ray properties change significantly across the remnant. In the following we present the statistical studies of the spectral fitting results.

(I) We got the spatial distribution of the absorbing column density (c.f. Fig. 4), as well as temperatures and ionization ages for the cool and hot components (c.f. Fig. 5). In order to show the large scale structures more clearly, we smoothed all these maps with a two-dimension Gaussian with FWHM  $40'' \times 40''$ , and overplotted the smoothed contours on these maps. The column density of the west part is higher than that of the east. This is consistent with the former studies (Keohane et al. 1996; Willingale et al. 2002), in which it was suggested that the absorption to the west is higher due to the interaction of the remnant with the molecular cloud. The column density lies in the range  $0.8 - 1.5 \times 10^{22} \text{ cm}^{-2}$  with the mean value of  $1.19 \times 10^{22} \text{ cm}^{-2}$ . The typical statistical error is  $\sim 5\%$  at 90% confidence level. The column density is a little smaller than  $1.50 \times 10^{22} \text{ cm}^{-2}$  derived by Willingale et al. (2002), but consistent with that from Keohane et al. (1996) given by the equivalent width of HI and OH ( $1.05 - 1.26 \times 10^{22} \text{ cm}^{-2}$ ).

The temperature distributions for the cool and hot components are not very similar. It seems that the higher temperature of the hot components appears at the out rim and Fe-rich regions (c.f. Fig 6). This is not surprising, since the hot component is responsible for most of the Fe K emission and also dominates continuum above 4 keV (Willingale et al. 2002).

The ionization age maps for both components are much similar to the corresponding ones given by Willingale et al. (2002). We can see that the map of the hot component is relatively uniform over the whole remnant, while the cool one shows some structures. The brightest shell, which has the largest density, doesn't have the highest ionization age. This leads to the conclusion that the brightest shell is later shocked. Considering that the cool component is associated with the reverse shock (Vink et al. 1996, Willingale et al. 2002), this suggests that the reverse shocked ejecta may be stratified and thus shocked at different time.

(II) We obtained the spatial distribution of all the elements concerned. The elemental abundance of each pixel is the mean of the two components weighted by their emission measures.

Figure 6 displays the abundance maps of Si, Ca and Fe. The contours have the similar meaning with those in Fig. 4. We can find that Si and possibly Ca abundances show a jet-like structure in the northeast and a counterpart in the southwest. This "jet" structure was first suggested by using the Si emission line equivalent width image (Hwang et al. 2000) and was confirmed with the ratio image of the Si He  $\alpha$  (plus continuum, 1.78  $\sim$  2.0 keV) and 1.3  $\sim$  1.6 keV (mostly weak Mg He  $\alpha$ , Fe L plus continuum) (Hwang et al. 2004). Our abundance maps further confirm their results. Meanwhile, from the Fe abundance map, we can find that Fe is relatively poor in the jet area but seems to be rich in the direction

perpendicular to it. It is also clearly shown in the map that the Fe-rich knots lie outside the Si- and S-rich ejecta, which is consistent with the results of Hughes et al. (2000) and Willingale et al. (2002).

(III) Figure 7 – 9 are the correlation plots of the abundances of Ne, Si, and Fe with the other elements. S abundance is strongly correlated with that of Si. Its correlation with other elements are very similar to those of Si, and are therefore not displayed. We note that the minimum points are excluded, for they represent regions which are dominated by the continuum emission and thus have no (or very weak) corresponding lines. In order to show the overall trends of the correlations more clearly, we binned the data points into 10 channels and overplotted them in the figures with big pentacles. The corresponding coherent coefficients are given in Table 1. Apparently Si is well correlated with S, as well as with Ca. There is also a good correlation between Ne and Mg.

We noticed that in the abundance correlation maps of Si versus Fe, there seems to be a two phase correlation with the break at Si abundance equaling to 3. When the Si abundance is lower than 3, there is a positive correlation with Fe, while negative when higher. All these features would give us information about the (explosive) nucleosynthesis of the SN, as will be discussed in detail in § 4.3.

(IV) The Doppler map (c.f. Fig. 4) we got is different from those of Willingale et al. (2002). They showed that the ejecta in the Southeast is generally blue shifted, while in the North red shifted. However, in our map, most regions are red shifted and only a small fraction in the Southeast are blue shifted. The Doppler map shows prominent “bar”-like features from the southeast to the northeast.

We found that the Doppler map is mostly the result of mis-calibration. The direction of the “bar”-like feature is exactly along the CCD columns. Since the CCD pixels in one column share one read-out circuit, the red shift “bar” is probably due to the inefficiency of the read-out circuit. The generally accepted velocity for the knots is in the order of 2000 km/s (Willingale et al. 2002), corresponding to an energy shift of  $\sim 15$  eV @ 2 keV (near the Si and S lines). However, the resolution of *Chandra*-ACIS is about an order of magnitude higher than this value. The calibration and/or the performance of *Chandra*-ACIS is probably not good enough to determine such a small energy shift. Therefore, we conclude that it is very difficult to derive a reliable Doppler map with the *Chandra*-ACIS data.

## 4 DISCUSSION

### 4.1 Jet structure

The ejecta structure and the explosion asymmetry of Cas A have been widely studied. It has been long suggested that the core-collapse SN explosion process is intrinsically asymmetric, from both the observational and theoretical point of

views (Khokhlov et al. 1999 and reference therein). For Cas A, it shows rapidly moving oxygen-rich material outside the nominal boundary (Fesen & Gunderson 1996) and evidence for two oppositely directed jets (Reed et al. 1999). The aspherical distribution of its ejecta suggests that the SN explosion, which produced Cas A, may be asymmetric.

Hwang et al. (2000, 2004) have further supported the jet emission of Si-rich ejecta using the *Chandra* data. These works are based on the equivalent width (EW) images of the corresponding emission lines. However the correlation between EW and the abundance can be distorted by temperature, column density and ionization age. In other words, the same abundance can be detected as significantly different EW because of the different line emissivity that is a function of the local plasma conditions. Willingale et al. (2002) gave the abundance maps from the *XMM-Newton* data, but the jet structure is not seen in their results, due to the spatial resolution limits and their bigger pixel size.

In this paper, we gave directly the element abundances map, among which Si, S and probably Ca show the jet structure as expected. The ejecta in the jet area are very enriched in Si, S and Ca, and relatively poor in Fe (still exists, c.f. Figure 3(B)). This confirms not only the presence of jet itself but also that these elements come from incomplete explosive Si-burning rather than O-burning (Khokhlov et al. 1999; Hughes et al. 2000). Meanwhile, the Fe in the counter-jet region (Figure 3(B)) is less enriched than the off-jet area (Figure 3 (C)), which also implies that the jet material did not emerge from as deep in the progenitor as other observed ejecta (Hughes et al. 2000 and reference therein).

## 4.2 Iron distribution

As far as we know,  $^{56}\text{Fe}$  mainly comes from the decay of  $^{56}\text{Ni}$ , which is synthesized in the (incomplete) explosive Si-burning. Hwang & Laming (2003) identified a region of nearly pure Fe ejecta, which might be a candidate for the site of  $\alpha$ -rich freezeout (see also Vink 2004). Early *Chandra* observation showed that the Fe emission in Cas A is associated with ejecta and mainly distributed in the faint region outside the bright Si-dominated shell in the east. The lack of Si beyond the Fe emission, as well as the lack of Fe inside the Si emission, argues against projection effects (Hughes et al. 2000).

From our abundance maps, we further confirmed that the ejecta which is highly enriched of Fe lies outside the Si and S dominated ejecta in the east. According to the onion model, the lighter an element is, the larger radius it should be located (Aschenbach 2002). As long as the projection effect may not play, at least an important role, this means that the ejecta in Cas A may have suffered some kind of overturn, either during or after the explosion. This overturn might

be the result of the neutrino-driven convection during the initiation of the SN explosion (Hughes et al. 2000).

In the previous *Chandra* results (Hwang & Laming 2003; Laming & Hwang 2003), it has been suggested that the Fe-rich ejecta have higher characteristic ionization age than the O/Si knots by factors of a few to 10, implying either a correspondingly higher density or an earlier shock time. As large density enhancement (or deficits) is subject to a number of hydrodynamic instabilities that might destroy the knots within a few shock crossing time scales (Klein et al. 1994; Klein et al. 2003; Wang & Chevalier 2001; Poludnenko et al. 2002; Poludnenko et al. 2004), such knots are thus not expected to be seen now. So Hwang & Laming (2003) claimed that early shock time and very modest (or no) density enhancement are the most consistent explanation for the Fe knots that have survived to be seen today. Comparing Figure 4 (middle panel) and the Fe abundance map in Figure 6, we can find that the Fe-rich knots in the southeast do have higher ionization age. This further confirms that they might be early shocked, and might be additional evidence for the overturn described previously.

### 4.3 Nucleosynthesis

In the range of about two orders of magnitude, the abundances of Si, S and Ca show tight correlations with each other (c.f. Fig. 8). Willingale et al. (2002) also presented the similar results using the *XMM-Newton* data and suggested this to be strong evidence for the nucleosynthesis of these elements by explosive O-burning and incomplete explosive Si-burning due to the shock heating of these layers in the core-collapse supernova. This kind of good correlation can also be found between abundances of Ne and Mg, which means that they might be the ashes of explosive C/Ne burning. All these results are generally consistent with the (explosive) nucleosynthesis theory of a massive star (Woosley et al. 2002; Woosley & Janka 2006).

Fe abundance is not correlated with any other element, with one exception that there seems to be a possible two phase correlation with Si (c.f. Fig. 8 or 9). It is contaminated by extremum data points, for it is difficult to reliably derive the Fe abundances from Fe-L lines (e.g. Suh et al. 2005). So we picked regions whose spectra show clearly Fe K lines, and re-draw the Si versus Fe abundance plot in Figure 10. Now the two phase correlation is more clearly presented. From Figure 6 we can easily find that the regions with Si abundance higher than 3 generally concentrate at the Si-dominated bright shell, which is natural, and also at the jet and its counterpart. These regions are believed to be the ejecta of incomplete explosive Si-burning or explosive O-burning. We know that explosive O-burning would lead to products with little or no Fe while in the incomplete explosive Si-burning Fe is one of the main products. From the

Si versus Fe correlation plot, we can see that Fe is not as enriched as Si, but still abundant. This would support that these ejecta mainly come from incomplete explosive Si-burning, but also mix with O-burning products. The regions with lower Si abundance are mainly the relatively faint parts of the remnant and might be dominated by the shocked circumstellar medium (CSM). We note here that the southeast ejecta, which are highly enriched in Fe and are believed to be synthesized in the complete explosive Si-burning, are only a small fraction of the total remnant. They don't affect much to the correlation we discussed above.

## 5 SUMMARY

We did a spatially resolved X-ray spectroscopy of SNR Cas A. An obvious jet structure can be found in the Si, S and Ca abundance maps, further confirming the former suggestions. However, the Fe map shows that it doesn't follow the jet, but distributes somehow perpendicular to it. Meanwhile, it lies outside the lighter elements (such as Si and S), which is consistent with the previous results and might be due to the neutrino-driven convection during the initiation of the SN explosion. The tight positive correlations of Si, S and Ca abundances (c.f. Figure 8) suggest that these elements come from explosive O-burning and incomplete Si-burning. Ne and Mg abundances also show a good positive correlation, which means that they should be the ashes of explosive C/Ne burning. The Fe abundance is positively correlated with that of Si when Si abundance is lower than 3 solar value, but when the Si abundance is higher, it appears a negative correlation. We propose this two phase correlation the result of the ways in which Fe is synthesized. The highly Si-enriched ejecta concentrated in the jet and the bright shell are probably a mixture of the explosive O-burning and the incomplete Si-burning products. The rest part, in contrast, might be dominated by the shocked CSM.

**Acknowledgements** We acknowledge the use of data obtained by Chandra. The Chandra Observatory Center is operated by the Smithsonian Astrophysical Observatory for and on the behalf of NASA. This work is supported by the National Science Foundation of China through grants 10533020 and 10573017.

## References

- Aschenbach B., 2002, in *Neutron Stars, Pulsars, and Supernova Remnants*, ed. Becker W., Lesch H., and Trümper J. (MPE Rep. 278; Garching: MPE), 13
- Arnaud K. A., 1996, *ASPC*, 101, 17
- Anders E., Grevesse N., 1989, *Geochimica et Cosmochimica Acta*, 53, 197
- Bleeker J. A. M., Willingale R., van der Heyden K. J. et al., 2001, *A&A*, 365, L225
- Borkowski K. J., Lyerly W. J., Reynolds S. P., 2001, *ApJ*, 548, 820
- Fesen, R. A., Hurford A. P., 1996, *ApJS*, 106, 563

**Table 1** coherent coefficient for data points excluding extremum ones.

Element	O	Ne	Mg	Si	S	Ca	Fe
O	-	0.33	0.41	0.33	0.26	0.14	0.13
Ne	0.33	-	0.49	0.19	0.16	0.05	0.25
Mg	0.41	0.49	-	0.48	0.39	0.16	0.24
Si	0.33	0.19	0.48	-	0.86	0.35	0.23
S	0.26	0.16	0.39	0.86	-	0.33	0.11
Ca	0.14	0.05	0.16	0.35	0.33	-	0.05
Fe	0.13	0.25	0.24	0.23	0.11	0.05	-

- Gotthelf E. V., Koralesky B., Rudnick L. et al., 2001, *ApJ*, 552, L39  
 Hughes J. P., Rakowski C. E., Burrows D. N. et al., 2000, *ApJ*, 528, L109  
 Hwang U., Holt S. S., Petre R., 2000, *ApJ*, 537, L119  
 Hwang U., Laming J. M., 2003, *ApJ*, 597, 362  
 Hwang U., Laming J. M., Badenes C. et al., 2004, *ApJ*, 615, L117  
 Keohane J. W., Rudnick L., Anderson M. C., 1996, *ApJ*, 466, 309  
 Klein R. I., Budil K. S., Perry T. S. et al., 2003, *ApJ*, 583, 245  
 Klein R. I., McKee C. F., Colella P., 1994, *ApJ*, 420, 213  
 Khokhlov A. M., Höflich P. A., Oran E. S. et al., 1999, *ApJ*, 524, L107  
 Laming J. M., 2001, *ApJ*, 546, L1149  
 Laming J. M., Hwang U., 2003, *ApJ*, 597, 347  
 McKee C. F., 1974, *ApJ*, 188, 335  
 Morrison R., McCammon D., 1983, *ApJ*, 270, 119  
 Nagataki S., Mizuta A., Yamada S. et al., 2003, *ApJ*, 596, 401  
 Poludnenko A. Y., Frank A., Blackman E. G., 2002, *ApJ*, 576, 832  
 Poludnenko A. Y., Dannenberg K. K., Drake R. P. et al., 2004, *ApJ*, 604, 213  
 Reed J. E., Hester J. J., Fabian A. C. et al., 1995, *ApJ*, 440, 706  
 Shklovsky I. S., 1973, *Soviet Astron.* 16, 749  
 Suh J. A., Audard M., Güdel M. et al., 2005, *ApJ*, 630, 1074  
 Thielemann F.-K., Nomoto K., Hashimoto M., 1996, *ApJ*, 460, 408  
 Thorstensen J.R., Fesen R.A., van den Bergh S., 2001, *AJ*, 122, 297  
 Vink J., Kaastra J.S., Bleeker J.A.M., 1996, *A&A*, 307, L41  
 Vink J., 2004, *New Astro. Rev.*, 48, 61  
 Wang C. Y., Chevalier R. A., 2001, *ApJ*, 549, 1119  
 Willingale R., Bleeker J. A. M., van der Heyden K. J. et al., 2002, *A&A*, 381, 1039  
 Woosley S. E., Heger A., Weaver T. A., 2002, *Rev. Mod. Phys.*, 74, 1015  
 Woosley S. E., Janka T., 2005, *Nat. Phys.*, 1, 147  
 Woosley S. E., Weaver T. A., 1995, *ApJS*, 101, 181  
 Zhang W., Woosley S. E., Heger A., 2004, *ApJ*, 608, 365

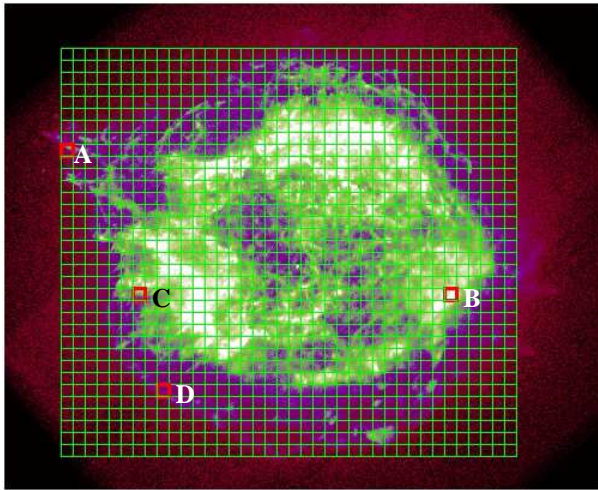


**Fig. 1** The pixel grid used in our analyses superimposed on the *Chandra* image of Cas A (Observation ID: 4639). Region A, B, C and D are described in § 3 and their spectra are presented in Fig. 3.

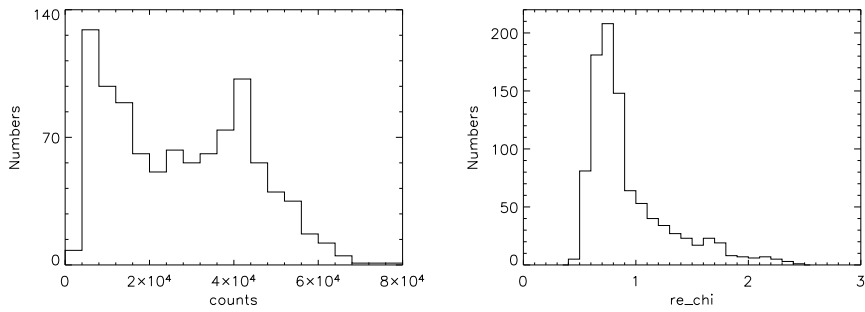


**Fig. 2** Frequency distributions of the 960 pixel counts (left panel) and  $\chi^2$  values obtained in the spectra fits (right panel).

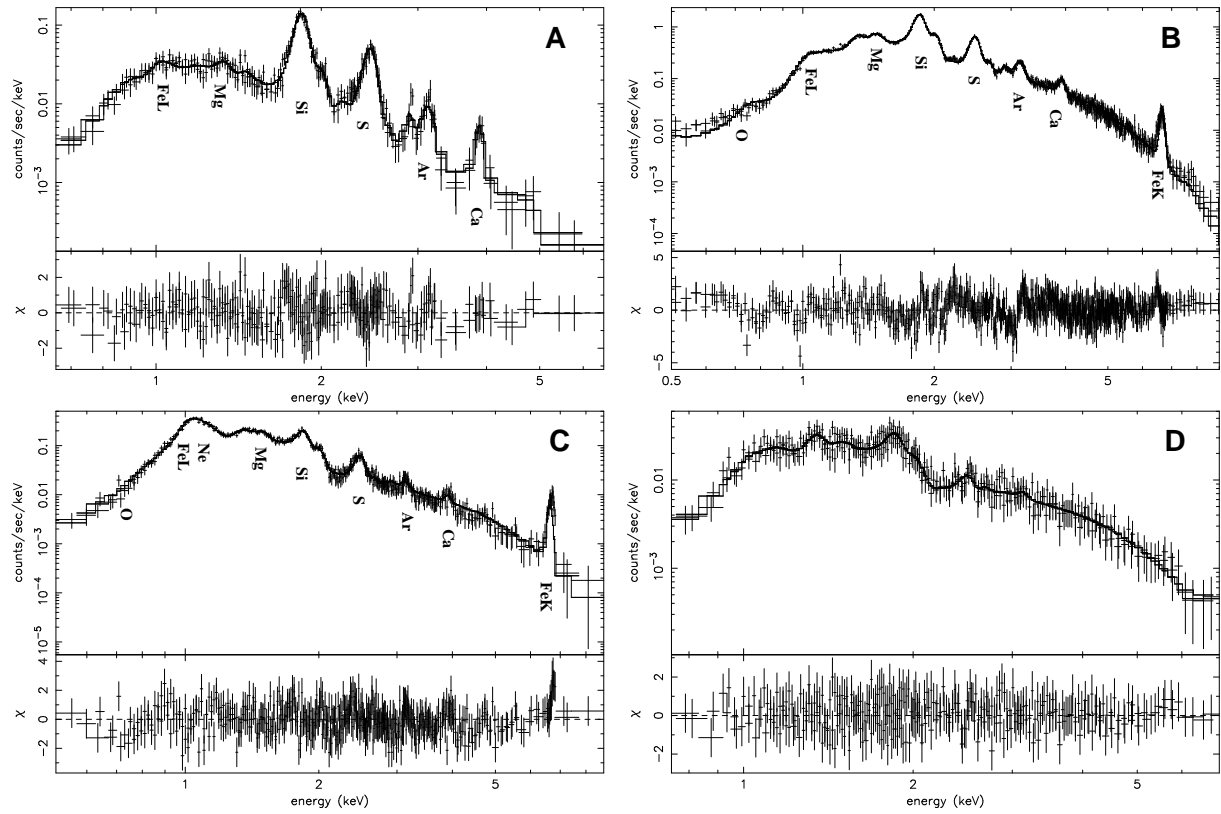


**Fig. 3** Spectra created from regions marked in Fig. 1. Spectrum A represents the spectrum of the explosive O-burning products, while B and C of incomplete and complete explosive Si-burning products respectively. Spectrum D is that of the forward shocked ISM.

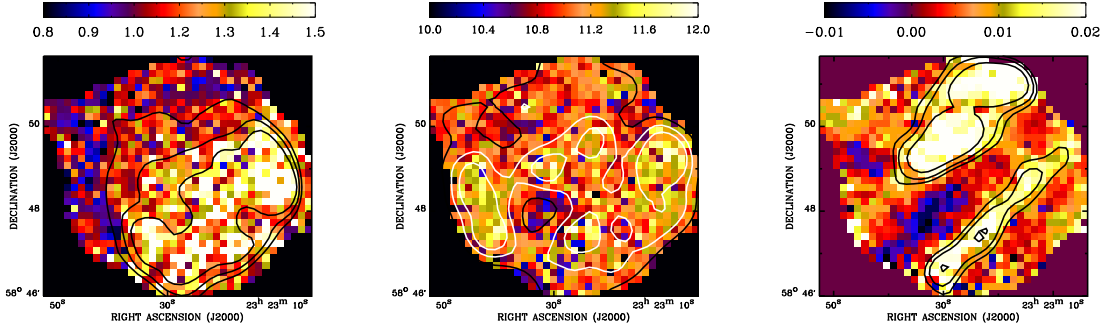


**Fig. 4** The absorbing column density ( $N_H$ ,  $10^{22} \text{ cm}^{-2}$ , left panel), ionization age ( $\text{Log}10 n_e t \text{ cm}^{-3} \text{ s}$ , middle panel), and red shift (right panel) maps of Cas A. The negative value of redshift means blueshift. The coding used is shown on the top of each panel. The overplotted contours represent the same dataset but smoothed by a two-dimension Gaussian component with FWHM of  $40'' \times 40''$ . The contour levels are as follows: 1.1, 1.2, 1.3 for  $N_H$ ; 11.0, 11.2, 11.3 for  $\text{Log}10 n_e t$ ; and 0.01, 0.012, 0.015 for redshift.

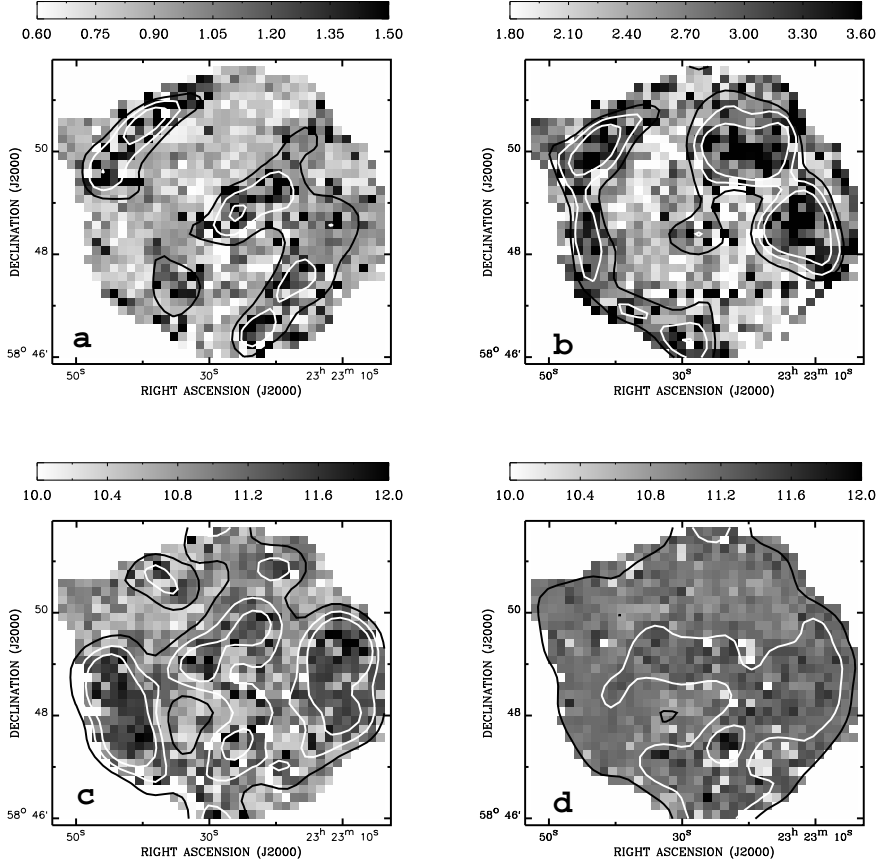


**Fig. 5** The maps of temperatures and ionization ages for the cool (index 1) and hot (index 2) components of Cas A. a:  $kT_1$  (keV), b:  $kT_2$  (keV), c:  $\text{Log}_{10}(n_e t)_1$  ( $\text{cm}^{-3} \text{s}$ ), d:  $\text{Log}_{10}(n_e t)_2$  ( $\text{cm}^{-3} \text{s}$ ). The contours represent the corresponding images smoothed by the same Gaussian component as used in Fig. 4. Contour levels are 1.0, 1.1, 1.2 for  $kT_1$ , and 2.6, 2.8, 3.0 for  $kT_2$ , while 11.0, 11.2, 11.3 for the two  $\text{Log}_{10}(n_e t)$ .

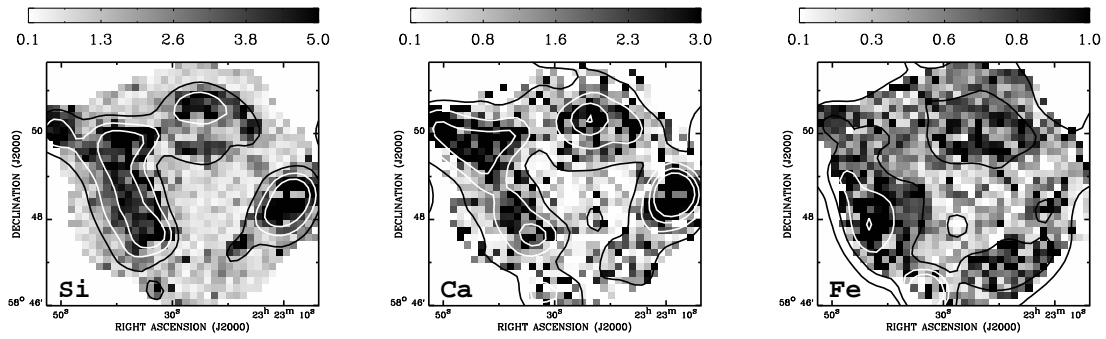


**Fig. 6** Si, Ca and Fe abundance (in units of solar abundance) maps of Cas A. Contours overlotted represent the same dataset but smoothed the same Gaussian component as used in Fig. 4. The contour levels are 2.0, 3.0, 4.0; 1.0, 2.0, 3.0, 4.0; and 0.3, 0.6, 0.9, 1.2 respectively.

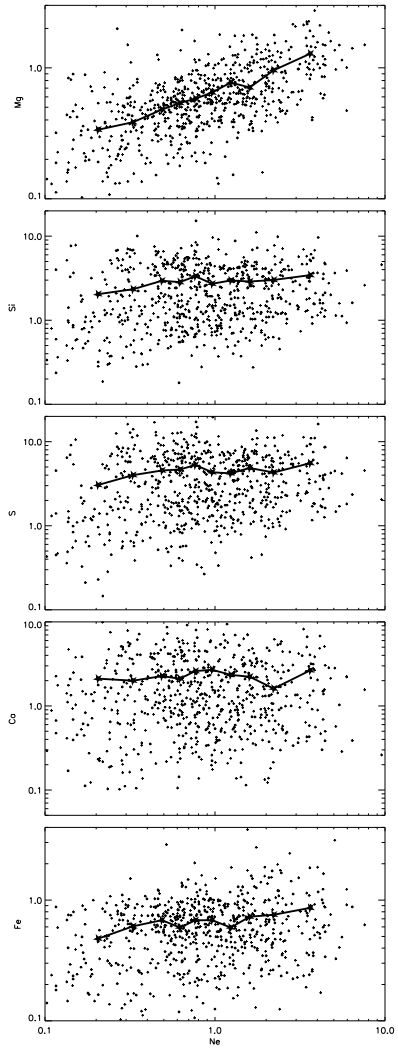


**Fig. 7** The abundance correlation plots between Ne and those of other elements. All the points were binned into 10 channels and overplotted in the figure with the big pentacles connected with the solid line.

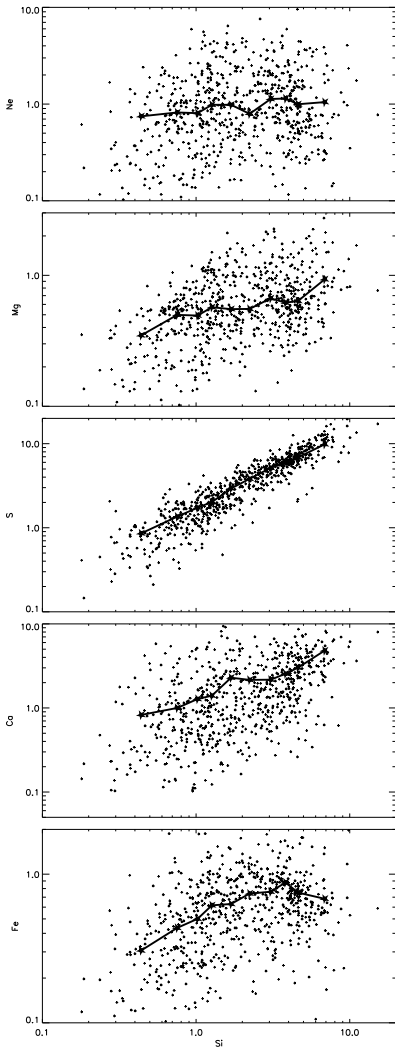


**Fig. 8** The Si abundance correlation plots versus those of other elements. The big pentacles and solid line have the same meaning as in Figure 7.

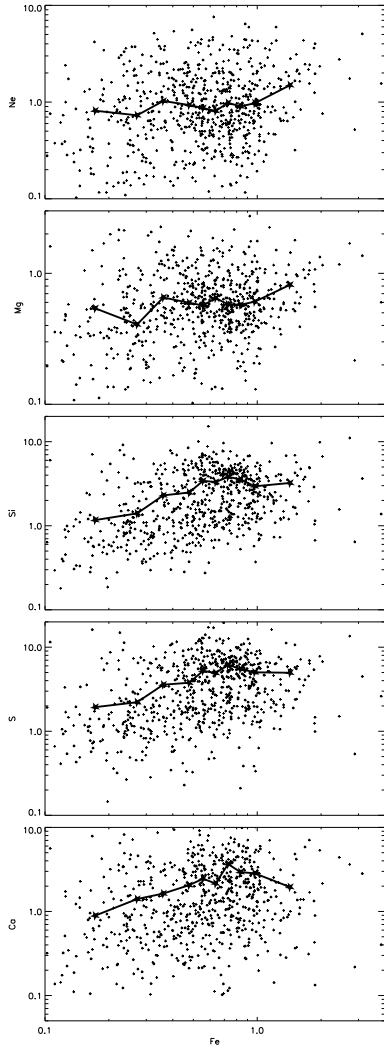


**Fig.9** The Fe abundance correlation plots versus those of other elements. The big pentacles and solid line have the same meaning as in Figure 7.

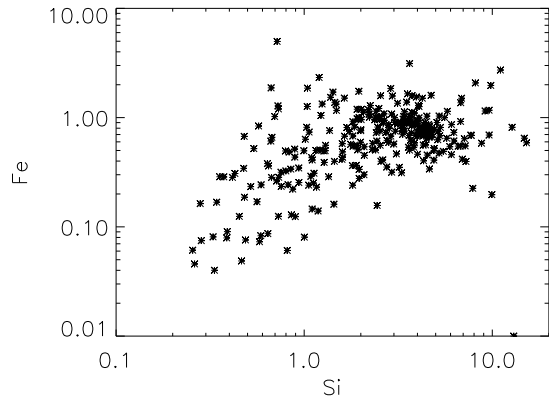


**Fig. 10** The Si versus Fe abundance correlation from regions with significant Fe-K lines.